Optics Letters

Spatiotemporal Bragg gratings forming inside a nonlinear dispersive medium

JUNCHI ZHANG,[1] W. R. DONALDSON,[2] AND GOVIND P. AGRAWAL[1,2,*]

[1] The Institute of Optics, University of Rochester, Rochester, New York 14627, USA
[2] Laboratory for Laser Energetics, University of Rochester, Rochester, New York 14623, USA
*govind.agrawal@rochester.edu

Received 31 July 2024; revised 18 September 2024; accepted 22 September 2024; posted 23 September 2024; published 8 October 2024

We show that a spatiotemporal Bragg grating can be created inside a nonlinear dispersive medium (such as silica fibers) by launching a periodic train of pump pulses that travel as fundamental solitons. We develop a theoretical model and use it to find the band structure of such gratings. We study the interaction of a probe pulse with the Bragg grating, both within and outside of momentum gaps. We also show that a photonic analog of the Anderson localization is possible when a disorder is introduced into a spatiotemporal Bragg grating.

https://doi.org/10.1364/OL.538147

Reflection and refraction of optical fields at a temporal boundary, with different refractive indices on its two sides, have attracted considerable attention in recent years [1–9]. A static temporal boundary is not easy to realize in practice as it requires a rapid change in the refractive index across the entire length of a suitable medium. A moving boundary, called a spatiotemporal boundary, was considered in a 2007 study [2]. A moving boundary was also used in Ref. [4] for studying the temporal reflection of optical pulses inside a dispersive waveguide such as an optical fiber. A spatiotemporal boundary can be realized in practice through a nonlinear index change induced by short pump pulses [10]. The temporal analog a Fabry–Perot interferometer is realized by launching two short pump pulses separated in time by a fixed delay [11].

When a train of short pump pulses is launched into a dispersive nonlinear medium, such as an optical fiber, it creates a periodic spatiotemporal modulation of the refractive index by increasing the index by a small amount (typically $<10^{-6}$) over the duration of each pump pulse. Such periodic index changes produce the spatiotemporal analog of a Bragg grating. Such a moving grating exhibits bandgaps in the momentum or **k** space, which are an analog of the frequency bandgaps occurring for a spatial Bragg grating. When a probe pulse, launched at a different wavelength, interacts with such a grating, it may be reflected or transmitted depending on whether its propagation constant (or wavenumber) lies inside or outside of a momentum gap. The temporal analog of a static Bragg grating has been discussed recently, without including the dispersive or the nonlinear effects of the medium [12]. It is expected that novel features would emerge when both the dispersive and nonlinear effects are included.

In this work, we investigate the interaction of probe pulses with a spatiotemporal Bragg grating, formed by a train of short pump pulses launched into an optical fiber, and include the effects of chromatic dispersion explicitly. The Kerr nonlinearity of a silica fiber increases its refractive index only over the duration of each pump pulse, resulting in a periodic index modulation that creates a Bragg grating, moving at the speed of pump pulses. We first present a mathematical model used to study the interaction of probe pulses with such a grating inside an optical fiber. We use it to discuss the band structure of spatiotemporal Bragg gratings and show that the frequency of the eigenmodes becomes imaginary in specific ranges of the wavenumber that correspond to the so-called momentum gaps. Such gaps exist whenever the refractive index of a material varies with time in a periodic fashion and have attracted considerable attention in the context of photonic time crystals [13–15]. Numerical simulations are used to reveal how the probe's evolution is modified by the presence of a spatiotemporal Bragg grating.

The formation of a spatiotemporal Bragg grating through the Kerr nonlinearity requires that the train of pump pulses maintain its structure (the shape, width, and interpulse spacing) during its propagation inside an optical fiber. This can be realized if the wavelength of pump pulses is chosen in the anomalous region, where the second-order dispersion parameter β_2 has a negative value, and their peak power is chosen such that each pump pulse propagates as a fundamental soliton. Moreover, solitons should be separated far apart enough that their nonlinear interaction is negligible. In this situation, the nonlinear index change induced by the Kerr effect varies with time as follows:

$$\delta n(t) = \frac{n_2 P_s}{A_{\text{eff}}} \sum_m \text{sech}^2\left(\frac{t - mT_d}{T_1}\right), \tag{1}$$

where n_2 is the Kerr coefficient, A_{eff} is the effective mode area of the fiber, and the sum is over all pulses within the soliton train. Each soliton of width T_1 has a "sech" shape, and two neighboring solitons are separated in time by T_d. The input peak power P_s of fundamental solitons is chosen such that $\gamma_s P_s T_1^2/|\beta_{2s}| = 1$, where the nonlinear parameter is defined as $\gamma_s = n_2\omega_s/(cA_{\text{eff}})$ [10].

To study how a moving Bragg grating, created by pump pulses, affects the propagation of a probe pulse launched at a different wavelength, we solve a standard nonlinear Schrödinger equation [10] describing the evolution of a weak probe pulse, but include its interaction with pump pulses through a cross-phase modulation term. The resulting equation is as follows [4]:

$$\frac{\partial A}{\partial z} + \Delta\beta_1 \frac{\partial A}{\partial t} + \frac{i\beta_2}{2}\frac{\partial^2 A}{\partial t^2} = \frac{2i\omega_0}{c}\delta n(t)A, \tag{2}$$

where $t = t_a - z/v_s$ is the reduced time in a moving frame, t_a is the actual time, and v_s is the velocity of solitons. The probe's envelope A is defined such that the electric field is given by $E(z,t) = \mathrm{Re}[A(z,t)\exp(i\beta_0 z - i\omega_0 t)]$, where the reference frequency ω_0 can be different from the probe's central frequency and β_0 is the corresponding propagation constant. The parameter, $\Delta\beta_1 = 1/v_g(\omega_0) - 1/v_s$, is related to the mismatch between the speed of the pump pulses and the group velocity at ω_0; β_2 is the dispersion parameter at ω_0. The factor of 2 on the right side of Eq. (2) results from index changes induced through the nonlinear phenomenon of cross-phase modulation (XPM) [10].

By choosing the reference frequency ω_0 suitably, we can eliminate the $\Delta\beta_1$ term in Eq. (2). This is achieved by utilizing the zero-dispersion wavelength of the fiber and choosing ω_0 as the frequency for which the speeds of pump and probe pulses become the same (two frequencies lie on opposite sides of the zero-dispersion wavelength). It is also useful to normalize Eq. (2) using two new variables: $\tau = t/T_d$ and $\xi = z(|\beta_2|/T_d^2)$. If we also use Eq. (1), we obtain the following equation:

$$\frac{\partial A}{\partial \xi} + \frac{i}{2}\frac{\partial^2 A}{\partial \tau^2} = \frac{iC_x}{\tau_1^2}\sum_m \mathrm{sech}^2\left(\frac{\tau - m}{\tau_1}\right)A(\xi,\tau), \tag{3}$$

where we have introduced two normalized parameters as follows:

$$C_x = \frac{2|\beta_{2s}|\omega_0}{\beta_2\omega_s}, \qquad \tau_1 = \frac{T_1}{T_d}. \tag{4}$$

The parameter C_x governs the XPM-induced coupling between pump and probe pulses Its value is close to 2 when $|\beta_{2s}|\omega_0 \approx \beta_2\omega_s$. In the following analysis, we choose $C_x = 2$. The parameter τ_1 represents the duty cycle of the train of pump pulses. Typically, τ_1 is ~0.1 because the width of pump pulses should be a small fraction of their pulses' separation.

We first use Eq. (3) to find the band structure of spatiotemporal Bragg gratings created by pump pulses. This equation has the same mathematical form as the Schrödinger equation for an electron moving in a periodic potential. We can thus utilize the Bloch theorem to find its solution. To be specific, we find solutions of Eq. (3) in the following form:

$$A(\xi,\tau) = e^{i(\kappa\xi - \Omega\tau)}\bar{A}(\tau), \tag{5}$$

where $\bar{A}(\tau)$ is a periodic function of τ (with period 1 in our normalized units) and κ is the Bloch wavenumber. For a given value of κ, we solve the eigenvalue equation for $\bar{A}(\tau)$ numerically to find the eigenvalues Ω, which may be real or complex. Solutions with real Ω correspond to propagating states, while those with complex Ω represent evanescent states. For a specific κ, two Ω values are possible that have opposite signs but the same magnitude as the potential is symmetric in τ.

We used two reasonable values of τ_1 for the results shown in Fig. 1, where the real and imaginary parts of Ω are plotted as a function of κ. We used the combination $\kappa\tau_1^2/2$ because its value of 1 corresponds to the barrier height produced by each soliton. As seen in Fig. 1, the real part of Ω vanishes in certain ranges of κ. As Ω becomes imaginary, these regions correspond to momentum gaps (in the moving frame used here).

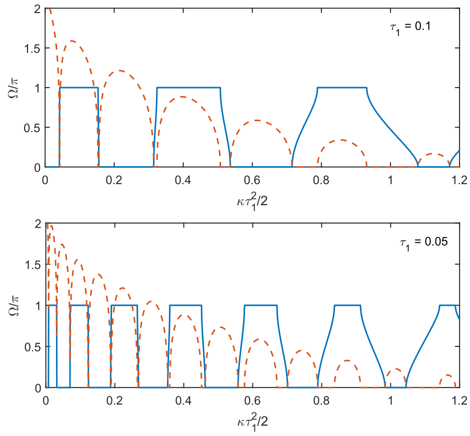

Fig. 1. Band structure of a spatiotemporal Bragg grating formed by a soliton train with $\tau_1 = 0.1$ (top) or 0.05 (bottom). The real (solid line) and imaginary (dashed line) parts of Ω are plotted as a function of κ. Momentum gaps are the regions where the real part of Ω vanishes.

The number of momentum gaps depends on the value of τ_1 and increases as τ_1 is reduced. For a given value of τ_1, the width of gaps depends on the value of κ. The width of propagation bands is smaller for low values of κ. This can be understood by noting that the "energy" is lower compared to the barrier height of each soliton under such conditions. For larger values of κ, propagation bands become large compared to the momentum gaps. This is because each soliton has a smaller reflectivity for the wave, and forming a bandgap requires interference between multiple reflections. When comparing the band structures for different τ_1, we see that a larger τ_1 results in a smaller separation between different bands, and each bandgap is smaller.

We next study how a probe pulse interacts with the spatiotemporal Bragg grating formed by a soliton train. Whereas the band structure was calculated for an infinite pulse train, we can only use a finite number of pulses in our simulations. For a finite pulse train, the first and last pulses act as temporal interfaces. The probe pulse must interact with the grating through one of these interfaces.

Figure 2 shows the results obtained by solving Eq. (3) numerically for a Gaussian probe pulse launched with the initial amplitude:

$$A(0,\tau) = \exp\left[-\frac{(\tau - \tau_s)^2}{2\tau_0^2} - i\Omega_i\tau\right], \tag{6}$$

with $\tau_0 = 10$, $\tau_s = -45$, and $\Omega_i = 7.63\pi$. The pump train contained 21 pulses, spaced such that $\tau_1 = 0.1$ and confined to the region marked by vertical dashed lines in the top panel of Fig. 2, showing the temporal evolution of the probe pulse with distance. The bottom panel displays the spectral evolution of this pulse.

As seen in Fig. 2, the probe pulse is initially far from moving Bragg grating formed by the soliton train. As it travels faster than pump pulses, it begins to interact with the grating at a distance $\xi = 1$ through the left temporal interface located at $\tau = -10$. For the situation shown in Fig. 2, κ of the incident pulse, $\kappa_i = \Omega_i^2/2$, is determined by the dispersion relation of the homogeneous medium. For our choice of Ω_i, κ_i falls in the momentum gap of the Bragg grating. This is the reason why the probe pulse is

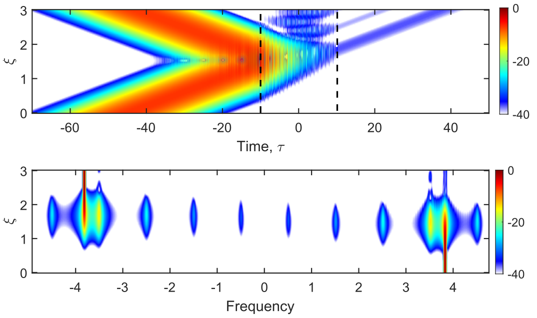

Fig. 2. Total reflection of a probe pulse when κ falls inside a momentum gap. The top and bottom panels show, respectively, the temporal and spectral evolutions with distance.

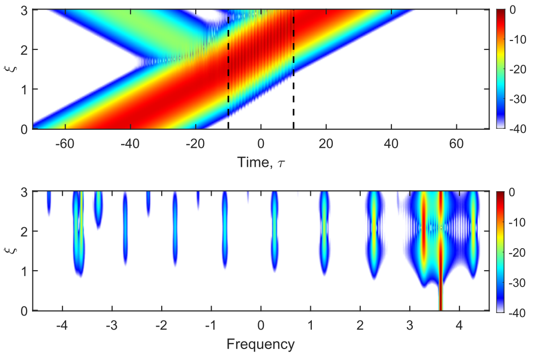

Fig. 3. Nearly total transmission of a probe pulse when κ is outside a momentum gap. The top and bottom panels show, respectively, the temporal and spectral evolutions with distance.

totally reflected in the top panel of Fig. 2. As the grating that we consider is moving at the speed of pump pulses, its "Bragg condition" is very different from the Bragg condition of a spatial grating. We discuss this point in detail in the Supplement 1.

We expect the probe pulse to be mostly transmitted through the Bragg grating if its κ value falls outside of a momentum gap. We can adjust κ by simply changing the initial frequency shift Ω_i of the probe pulse. Figure 3 shows the temporal and spectral evolutions of probe pulse using the same parameter values except for $\Omega_i = 7.23\pi$. As expected, the probe pulse is mostly transmitted through the Bragg grating. A small amount of energy (about 3%) is reflected because of a mismatch between the modes propagating inside and outside of the Bragg-grating region.

Spectral evolution is also different in the preceding two cases. As the probe begins to interact with the moving Bragg grating, multiple equally spaced sidebands are generated in both cases. However, the probe's frequency undergoes a large spectral shift only in the total-reflection case shown in Fig. 2. A much smaller spectral shift occurs when the probe is nearly transmitted through the Bragg grating.

To understand the origin of such spectral shifts, it is useful to unfold the band structure of a spatiotemporal Bragg grating, as shown by the staircase-like curve in Fig. 4. Dispersion in the region outside of the grating is shown by the dashed parabolic curve. Vertical (red) solid lines represent the spectrum of the probe pulse, while the horizontal (blue) solid lines denote the range of κ for the probe pulse. Vertical (red) dashed lines mark the spectral shift occurring when the probe pulse is transmitted

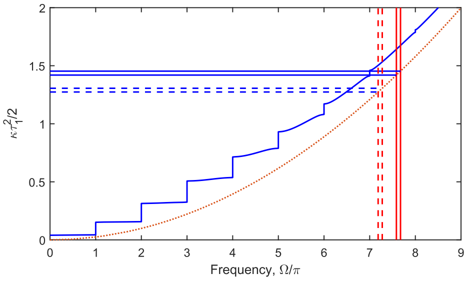

Fig. 4. Unfolded band structure of a spatiotemporal Bragg grating. The dispersion in the region outside of the grating is shown by a dashed curve. Vertical and horizontal lines mark the spectral and κ ranges.

through the grating. In the case of nearly total reflection of the incident pulse, the spectral shift becomes much larger because Ω becomes negative. Some energy is still transmitted through the grating even in this case because of a finite number of solitons used to form the Bragg grating.

To relate our theory to experiments, we estimate the physical values for the parameters used in our simulations. To suppress undesired higher-order nonlinear effects, one may choose T_1 = 1 ps and T_d = 10 ps. In this case, the Bragg grating is formed by using 1.7-ps-wide pump pulses separated by 10 ps. Using a realistic value, $|\beta_2| = 20\,\mathrm{ps}^2/\mathrm{km}$, at the 1550-nm wavelength for a silica fiber, the normalized length $\xi = 1$ corresponds to 5 km. Thus, experiments will require several kilometers of fiber, a length that is not unrealistic. As for the probe's wavelength, its group velocity should be close to that of pump pulses. One choice is 1145 nm in the normal-dispersion region of silica fibers, which have their zero-dispersion wavelength near 1300 nm.

So far, we have assumed a periodic soliton train, which creates a perfect Bragg grating. Just as electrons can exhibit "Anderson localization" in disordered crystals, a photonic analog of this concept has been found to occur for several optical devices [16–18]. Here we investigate whether it occurs for spatiotemporal Bragg gratings formed by a disordered train of solitons, when the grating is assumed to be long enough that its boundaries have no effect on the probe's evolution.

Although a disorder can be created by randomizing variables such as each soliton's amplitude, width, or phase, here we focus on the disorder caused by random variations in pulse-to-pulse spacing. Mathematically, we replace the $\tau - m$ in Eq. (3) with $\tau - m - x_m$, where x_m varies in a random fashion with the integer m. We used a uniform distribution for x_m in the interval $[-0.05, 0.05]$. We solved for the eigenstates of Eq. (3) for the choice $\tau_1 = 0.05$ and found that a localized state exists when the Bragg grating is not perfectly periodic. Figure 5 shows such a localized eigenstate. The value of κ for this state, $\kappa\tau_1^2/2 = 1.087$, lies in the propagation band of a perfect Bragg grating (see Fig. 1).

The localized nature of the eigenstate in Fig. 5 is the result of the disorder introduced in the soliton train. In the frequency domain, the spectrum has two widely separated dominant peaks. This feature indicates that the localized state contains two waves propagating in the opposite directions. The fine oscillatory structure in the time domain results from the interference of these two waves.

We performed numerical simulations to study how the Anderson-type localization affects the evolution of a probe

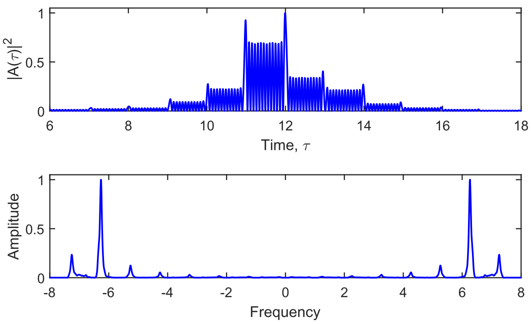

Fig. 5. Localized eigenstate of a disordered Bragg grating in the time and frequency domains.

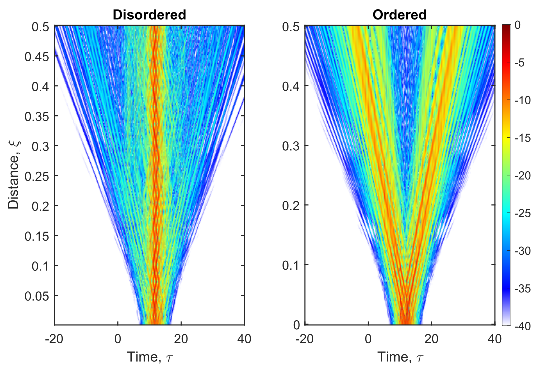

Fig. 6. Evolution of a probe pulse in a disordered (left) and a perfect (right) Bragg grating showing localization in the former case.

pulse. Since the localized mode mainly consists of two frequencies, we launch a Gaussian pulse that contains two spectral components and use the following form at the input end:

$$A(0, \tau) = \exp\left[-\frac{(\tau - \tau_s)^2}{2\tau_0^2}\right]\cos(\Omega_i \tau). \tag{7}$$

The parameters are chosen such that this pulse has a shape similar to the localized mode shown in Fig. 5: $\tau_s = 11.7, \tau_0 = 1.9$, and $\Omega_i = 12.5\pi$. Figure 6 compares the pulse's evolution in the disordered and perfect cases. In a disordered grating, most of the pulse's energy remains localized at its initial position because of its coupling to the localized mode shown in Fig. 5. Some energy radiates away because of a mismatch between the input pulse shape and the localized mode.

It is interesting to compare this type of evolution with a Bragg grating without any disorder. As seen in Fig. 6, when the disorder is not present, the input probe pulse excites two propagating modes of the crystal. The two frequency components of the input pulse break into two pulses that travel at different speeds, each experiencing dispersion-induced broadening with propagation. We conclude that it should be possible to observe localization of the probe pulse by launching a disordered train of pump pulses.

In conclusion, we have shown that a spatiotemporal Bragg grating can be created inside a dispersive nonlinear medium by launching a periodic train of pump pulses that travel as fundamental solitons. We developed a theoretical model and used it to find the band structure of such gratings and to study the interactions of probe pulses with the Bragg grating, both within and outside of momentum gaps. We found that a photonic analog of Anderson localization can occur when a disorder is introduced into a spatiotemporal Bragg grating.

We briefly comment on how our device differs from photonic time crystals that have attracted considerable recent attention [13–15]. Their most striking feature is the possibility of parametric amplification. For spatiotemporal Bragg gratings studied here, parametric amplification is not possible because the total number of photons is expected to be conserved. In our case, the nonlinear index change produced by pump pulses is relatively small. Moreover, backward propagation does not occur in devices proposed here.

Acknowledgment. This material is based upon the work supported by the Department of Energy (National Nuclear Security Administration) and the University of Rochester "National Inertial Confinement Fusion Program" under Award Number DE-NA0004144.

Disclosures. The authors declare no conflicts of interest.

Data availability. Data underlying the results may be obtained from the authors upon reasonable request.

Supplemental document. See Supplement 1 for supporting content.

REFERENCES

1. J. Mendonça and P. Shukla, Phys. Scr. **65**, 160 (2002).
2. F. Biancalana, A. Amann, A. V. Uskov, *et al.*, Phys. Rev. E **75**, 046607 (2007).
3. Y. Xiao, D. N. Maywar, and G. P. Agrawal, Opt. Lett. **39**, 574 (2014).
4. B. Plansinis, W. Donaldson, and G. Agrawal, Phys. Rev. Lett. **115**, 183901 (2015).
5. B. W. Plansinis, W. R. Donaldson, and G. P. Agrawal, J. Opt. Soc. Am. B **35**, 436 (2018).
6. C. Caloz and Z.-L. Deck-Léger, IEEE Trans. Antennas Propag. **68**, 1569 (2020).
7. J. Zhang, W. Donaldson, and G. Agrawal, J. Opt. Soc. Am. B **38**, 997 (2021).
8. J. Zhang, W. Donaldson, and G. P. Agrawal, J. Opt. Soc. Am. B **39**, 1950 (2022).
9. J. Zhang, W. Donaldson, and G. P. Agrawal, Phys. Rev. A **107**, 063518 (2023).
10. G. P. Agrawal, *Nonlinear Fiber Optics*, 6th ed (Academic Press, 2019).
11. J. Zhang, W. Donaldson, and G. P. Agrawal, J. Opt. Soc. Am. B **38**, 2376 (2021).
12. S. F. Koufidis, T. T. Koutserimpas, and M. W. McCall, Opt. Lett. **48**, 4500 (2023).
13. E. Galiffi, R. Tirole, S. Yin, *et al.*, Adv. Photonics **4**, 014002 (2022).
14. Y. Sharabi, A. Dikopoltsev, E. Lustig, *et al.*, Optica **9**, 585 (2022).
15. M. M. Asgari, P. Garg, X. Wang, *et al.*, "Photonic time crystals: theory and applications," arXiv (2024).
16. M. Segev, Y. Silberberg, and D. N. Christodoulides, Nat. Photonics **7**, 197 (2013).
17. A. Mafi, Adv. Opt. Photonics **7**, 459 (2015).
18. A. Yamilov, S. E. Skipetrov, T. W. Hughes, *et al.*, Nat. Phys. **19**, 1308 (2023).